JOURNAL OF SPACECRAFT AND ROCKETS
Vol. 38, No. 6, November–December 2001

Dynamic Behavior of a Tethered System with Multiple Subsatellites in Elliptic Orbits

Noboru Takeichi*
University of Tokyo, Tokyo 113-8654, Japan
and
M. C. Natori† and Nobukatsu Okuizumi‡
Institute of Space and Astronautical Science, Kanagawa 229-8510, Japan

Dynamic behavior of a tethered system with multiple subsatellites subjected to both atmospheric drag and changes of gravity gradient in elliptic orbits is investigated. The tethered system is modeled as a combination of rigid-body subsatellites and lumped tether masses, and flexibility of the tether is considered. The results of the numerical experiments show that the libration of the total system can diverge due to the atmospheric drag, and the total system begins tumbling motion later. The physical interpretation is clearly presented by focusing on the deviation from the periodic motion. Effects of the atmospheric drag on the attitude motions of the subsatellites and the tension states of the tether are also investigated. It is shown that the large perturbations can cause partial slack states of the tether, which causes unstable attitude motions of some of the subsatellites.

Nomenclature

C_d	=	drag coefficient
c	=	damping coefficient of tether, N · s/m
d	=	diameter, m
E	=	Young's modulus of tether, N/m^2
e	=	orbital eccentricity
F	=	atmospheric drag, N
h_{peri}	=	perigee altitude, m
I_x, I_y, I_z	=	inertia of subsatellite, kg · m^2
k	=	spring constant, N/m
l	=	length of tether element, m
l_e	=	effective length for F, m
l_n	=	natural length of l, m
M	=	mass, kg
r	=	orbital radius, m
r_E	=	Earth radius, m
r_{peri}	=	orbital radius at perigee, $r_{\text{peri}} \triangleq r_E + h_{\text{peri}}$, m
T	=	tension of tether, N
T_q	=	external torque of subsatellite, N · m
V	=	relative velocity, m/s
x, y, z	=	position of lumped tether mass or a subsatellite in the orbital coordinates, m
Δl	=	deflection of tether, m
λ	=	stability parameter
μ	=	Earth gravitational constant, m^3/s^2
ν	=	true anomaly measured from perigee, rad
ρ	=	atmospheric density, kg/m^3
ψ	=	pitch angle of subsatellite, rad
Ω	=	Earth angular velocity, rad/s

Subscripts

p	=	periodic motion
s, a, b, c, d	=	subsatellites
T	=	total system
t	=	tether
0	=	initial conditions

Received 28 December 2000; revision received 1 June 2001; accepted for publication 22 June 2001.

*Graduate Student, Department of Aeronautics and Astronautics, 7-3-1 Hongo, Bunkyo-ku; takeichi@taurus.eng.isas.ac.jp. Student Member AIAA.

†Professor, Spacecraft Engineering, 3-1-1 Yoshinodai, Sagamihara. Associate Fellow AIAA.

‡Research Associate, Spacecraft Engineering, 3-1-1 Yoshinodai, Sagamihara.

Introduction

MANY applications of tethered systems have been proposed because tethers can be used to construct large-scale space structure systems. A tethered system with multiple subsatellites shown in Fig. 1 has been proposed to observe the atmospheric region from 150 to 500 km (Ref. 1). The system consists of one large mother satellite and four small observer satellites connected to the mother satellite by one tether, and it can observe multiple regions simultaneously. Because the purpose of this system is to observe the atmosphere, its orbital speed is reduced by atmospheric drag; therefore, a high-energy orbit is necessary to execute a long-term operation. Because the observation altitude is limited, the system should utilize an elliptic orbit. Thus, this tethered system is subjected to various changes of gravity gradient and atmospheric environment.

Dynamic behavior of a tethered system subjected to aerodynamic forces in circular orbits has been investigated using simplified models,[2,3] and the stability of the equilibrium state has been investigated analytically. It has been shown that the equilibrium states can be unstable due to the combined effects of tether elasticity and atmospheric density gradient. The stability criteria of parameters (such as mass of the subsatellite and length of the tether and atmospheric drag) have been presented considering the mass of the tether and the atmospheric drag acting on it[4]; the stability criteria in slightly eccentric [$e = 1.5(10^{-4})$–$1.5(10^{-3})$] and nonequatorial orbits have also been investigated.[5] Parametric investigations show that stability criteria in a slightly eccentric orbit are almost the same as those in a circular orbit.

In elliptic orbits, tethered systems begin tumbling and libration due to the changes of gravity gradient and orbital angular velocity. Because the equations of motion of even a simplified tethered system become highly nonlinear, and the equilibrium state cannot be obtained, numerical methods to analyze nonlinear systems have been applied. Periodic solutions and their stability have been analyzed numerically,[6,7] and it has been shown that stable libration of a tethered system is possible in elliptic orbits when $e < 0.353$. Through methods such as Poincaré maps, bifurcation diagrams, and Lyapunov exponents, motions of a tethered system have been classified into libration and tumbling.[8–11] It has been shown that motions are determined by eccentricity, tether elasticity, and initial conditions. It has also been shown that the criteria of initial conditions,

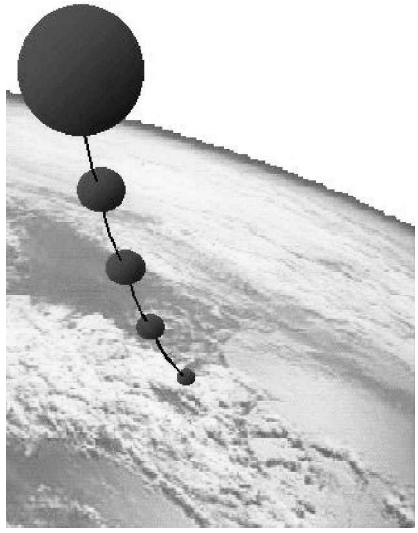

Fig. 1 Image of a tethered system for atmospheric observation.

which lead a tethered system to continue libration, become more severe as the eccentricity increases.

Attitude motions of subsatellites in the station-keeping phase have also been investigated. The in-plane dynamics of a rigid-body subsatellite has been discussed neglecting tether mass and flexibility and assuming constant tether tension,[12] and the coupling of tether lateral vibration and attitude motion has been investigated analytically.[13] The amplitude of satellite attitude motion was to be very small in the station-keeping phase. In these studies, no external forces such as atmospheric drag was considered, and only the case of circular orbit was discussed. Active and passive controls of three-dimensional attitude motion of the subsatellite by using a reaction wheel and aerodynamic equipment were discussed.[14] The attitude motion was shown to be stable about the three axes; neither flexibility of the tether nor the aerodynamic forces on it has been considered.

This study intends to clarify the fundamental characteristics of dynamic behavior of tethered systems subjected to atmospheric drag in elliptic orbits. A relatively complete model of a tethered system, where distributed mass, flexibility of the tether, and atmospheric drag on it are considered, is used in numerical simulations to investigate dynamic behavior. It is considered that tumbling motions of the total system and slack state of the tether, in which structural characteristics of the tether are lost, can cause operations and scientific observations to be infeasible. Therefore, the characteristics of librations of the tethered system and tension states of the tether, facing atmospheric drag and changes of gravity gradient and orbital angular velocity, are the focus. In the investigations, a tethered system with single subsatellite (TSS) is used to clarify the fundamental characteristics first. Second, results of a tethered system with multiple subsatellites (TMS) are compared with those of the TSS.

Formulation

System Configurations and Assumptions

The mathematical model of the tethered systems is shown in Figs. 2 and 3. The TSS consists of a subsatellite and a mother satellite connected by one tether, and the TMS consists of four subsatellites and a mother satellite connected by one tether. The purpose of this study is to clarify the effects of the atmospheric drag and the orbital eccentricity on dynamics of the tethered system for a long duration. Because the relative motions of the satellites and tethers are the focus, the orbital perturbations due to atmospheric drag and librations should be ignored. By letting the mother satellite be in an elliptic orbit without any perturbations, we can focus on only the relative motions of the satellites and tethers. The assumption to ignore the orbital perturbations corresponds to the system having some orbital control functions. In actual systems, the dynamics of the system is affected by orbital controls, atmospheric drag, and so on. In this paper, the effects of the atmospheric drag are clarified. The following assumptions are made: 1) The orbital motion is decoupled with

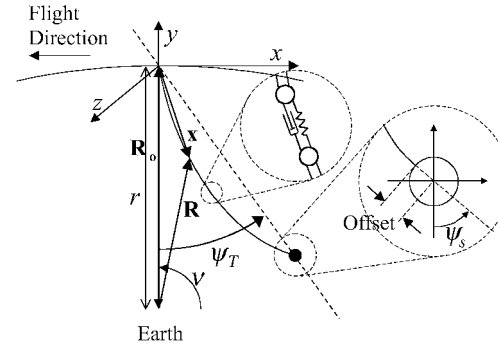

Fig. 2 Coordinates of system.

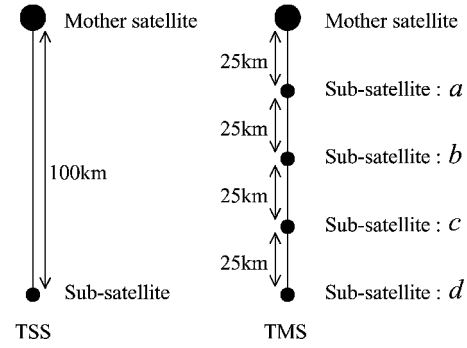

Fig. 3 Configurations of TSS and TMS.

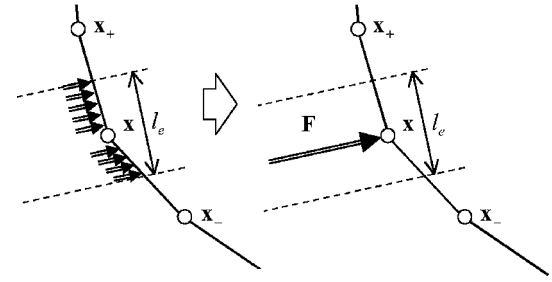

Fig. 4 Assumption of atmospheric drag on tether.

the attitude motion of the tethered system. 2) The center of mass is moving in an equatorial orbit around the spherical Earth. 3) Only in-plane motion is considered because the characteristic feature of gravity-gradient change and atmospheric drag affect mainly in-plane motion. 4) The subsatellites are spherical rigid bodies, and they are attached to the tether with offsets. 5) The mother satellite coincides to the origin of the orbital coordinate system. 6) The tether is modeled as lumped masses connected by combinations of a spring and a dashpot, which are shown as white circles in Figs. 2 and 4. Through this model, the characteristics of the tether, such as flexibility, distributed mass, and no bending rigidity, are considered. 7) The tether is initially fully deployed, and active controls of the tethered system are not considered. 8) The atmosphere rotates with the Earth, and its density is a function only of altitude. 9) The distributed atmospheric drag on tether elements is concentrated at mass points, lumped mass of the tether or the subsatellites. 10) To focus on the dynamics of the tethered system subjected to the atmospheric drag and changes of orbital angular velocity and gravity gradient, the orbital perturbation due to the atmospheric drag is not considered. Through this model, deflection and slack state of the tether, distributed atmospheric drag on it, and attitude motions of the subsatellites can be investigated.

Equations of Motion

Lagrange Equations

Equations of motion are obtained by using the Lagrange formulation. Let $\boldsymbol{x}$ and $\boldsymbol{R}$ be the position vectors of a mass point in the orbital frame and in the inertial frame, respectively, and $\boldsymbol{R}_0$ be the position vector of the center of mass of the total tethered system as

shown in Fig. 2. The following equations can be obtained for the position and the velocity of the point mass:

$$\boldsymbol{R} = \boldsymbol{R}_0 + \boldsymbol{x} \tag{1}$$

$$\dot{\boldsymbol{R}} = \dot{\boldsymbol{R}}_0 + \dot{\boldsymbol{x}} + \dot{\boldsymbol{\nu}} \times (\boldsymbol{R}_0 + \boldsymbol{x}) = \begin{bmatrix} \dot{x} - \dot{\nu}(y+r) \\ \dot{y} + \dot{r} + \dot{\nu}x \\ \dot{z} \end{bmatrix} \tag{2}$$

The kinetic energy K and potential energy U can be expressed as follows denoting mass of the mass point as M:

$$K = \tfrac{1}{2}M\|\dot{\boldsymbol{R}}\|^2 \tag{3}$$

$$U = -\mu(M/\|\boldsymbol{R}\|) \tag{4}$$

The elastic potential energy P and dissipation function W of the mass point related to two neighboring mass points (denoted as $-$ and $+$, shown in Fig. 4) can be expressed as

$$P = \tfrac{1}{2}k(l_+ - l_n)^2 + \tfrac{1}{2}k(l_- - l_n)^2 \tag{5}$$

$$W = \tfrac{1}{2}c\dot{l}_+^2 + \tfrac{1}{2}c\dot{l}_-^2 \tag{6}$$

where

$$\boldsymbol{l}_+ = \boldsymbol{x}_+ - \boldsymbol{x}, \qquad \boldsymbol{l}_- = \boldsymbol{x} - \boldsymbol{x}_-, \qquad l = \|\boldsymbol{l}\|, \qquad \dot{l} = \frac{\mathrm{d}}{\mathrm{d}t}\|\boldsymbol{l}\| \tag{7}$$

The equations of the subsatellite of TSS and of the bottom subsatellite of TMS have no variables with suffix -.

Lagrangian L about the mass point is obtained as

$$L = K - U - P \tag{8}$$

and the Lagrange equations of motion can be obtained as follows:

$$\frac{\mathrm{d}}{\mathrm{d}t}\left(\frac{\partial \sum L}{\partial \dot{q}}\right) - \frac{\partial \sum L}{\partial q} + \frac{\partial \sum W}{\partial \dot{q}} = Q \tag{9}$$

Equations of Motion for Mass Points

After assuming $z = \dot{z} = 0$, we obtain the following equations of motion for the lumped tether masses and the subsatellites:

$$\begin{aligned}\ddot{x} = {} & \ddot{\nu}(y+r) + x\dot{\nu}^2 + 2\dot{\nu}(\dot{y}+\dot{r}) - \mu x\{x^2 + (y+r)^2\}^{-\frac{3}{2}} \\ & - \alpha_+[(T_+/M)(x - x_+)/l_+] \\ & - \alpha_-[(T_-/M)(x - x_-)/l_-] + F_x/M\end{aligned} \tag{10}$$

$$\begin{aligned}\ddot{y} = {} & -\ddot{r} - \ddot{\nu}x - 2\dot{\nu}\dot{x} + (y+r)\dot{\nu}^2 - \mu(y+r)\{x^2 + (y+r)^2\}^{-\frac{3}{2}} \\ & - \alpha_+[(T_+/M)(y - y_+)/l_+] \\ & - \alpha_-[(T_-/M)(y - y_-)/l_-] + F_y/M\end{aligned} \tag{11}$$

where

$$T = k(l - l_n) + c\dot{l} \tag{12}$$

$$k = \pi d_t^2 E \big/ 4l_n \tag{13}$$

$$c = 0.03 \times c_{\mathrm{cr}} = 0.03 \times 2 \times \sqrt{M_t k} \tag{14}$$

In Eq. (14), c is set to 3% of c_{cr}, which is the longitudinal critical damping coefficient of a single pendulum consisting of a tether element and a tether point mass. Variables α and $\boldsymbol{F}$ are based on the tether tension state and the atmospheric drag, respectively. To express that the tether cannot have compressive stress, the coefficient α is given as follows:

$$l \geq l_n \rightarrow \alpha = 1, \qquad l < l_n \rightarrow \alpha = 0 \tag{15}$$

The values of atmospheric drag on the tether and the subsatellites are as follows:

For lumped masses of the tether,

$$\boldsymbol{F} = \tfrac{1}{2}\rho_{(r,y)}C_{dt}d_t l_e \|\boldsymbol{V}\|\boldsymbol{V} \tag{16}$$

For the subsatellites,

$$\boldsymbol{F} = \tfrac{1}{2}\rho_{(r,y)}\left[C_{dt}d_t l_e + \left(\pi d_s^2 \big/ 4\right)C_{ds}\right]\|\boldsymbol{V}\|\boldsymbol{V} \tag{17}$$

where

$$\boldsymbol{V} = \begin{bmatrix} (\dot{\nu} - \Omega)(r+y) - \dot{x} \\ -\dot{y} - \dot{r} \end{bmatrix} \tag{18}$$

$$l_e = \frac{1}{2}\left[\|\boldsymbol{l}_-\|\sqrt{1 - \left(\frac{\boldsymbol{l}_- \cdot \boldsymbol{V}}{\|\boldsymbol{l}_-\|\|\boldsymbol{V}\|}\right)^2} + \|\boldsymbol{l}_+\|\sqrt{1 - \left(\frac{\boldsymbol{l}_+ \cdot \boldsymbol{V}}{\|\boldsymbol{l}_+\|\|\boldsymbol{V}\|}\right)^2}\right] \tag{19}$$

Attitude Motion of Subsatellites

Attitude angles of the subsatellites are measured from the local vertical shown in Fig. 2. The equation for ψ_s is given as follows for spherical subsatellites:

$$\begin{aligned}\ddot{\psi}_s &= -\ddot{\nu} - [(I_x - I_y)/I_z]/(3\mu/r^3)\cos\psi_s \sin\psi_s + T_q/I_z \\ &= -\ddot{\nu} + T_q/I_z\end{aligned} \tag{20}$$

where

$$T_q = T_+(d_s/2)\sin(\phi_+ - \psi_s) + T_-(d_s/2)\sin(\phi_- - \psi_s) \tag{21}$$

$$\phi_\pm = \tan^{-1}[(x - x_\pm)/(y_\pm - y)] \tag{22}$$

Orbital Motion

The equations of orbital motion are obtained as follows:

$$\ddot{r} = r\dot{\nu}^2 - \frac{\mu}{r^2} + \frac{1}{M_T}\sum \mu M \frac{3(x^2 + 3y^2)}{2r^4} + \frac{Q_r}{M_T} \tag{23}$$

$$\begin{aligned}&\left\{M_T r^2 + \sum M(x^2 + y^2)\right\}\ddot{\nu} = -2M_T\dot{r}r\dot{\nu} \\ &\quad - \sum M\{2\dot{\nu}(x\dot{x} + y\dot{y}) + \ddot{x}y + 2\dot{x}\dot{y} + x\ddot{y}\} + Q_\nu\end{aligned} \tag{24}$$

When x^2/r^2 and $y^2/r^2 \cong 0$ are assumed and the orbital perturbation is neglected, the orbital equations are well approximated as follows:

$$\ddot{r} = r\dot{\nu}^2 - \mu/r^2 \tag{25}$$

$$\ddot{\nu} = -2\dot{\nu}\dot{r}/r \tag{26}$$

System Parameters

When a feasible tethered system is considered to fit the atmospheric observation program, constants for the analysis shown in Tables 1 and 2 are selected. The subsatellites of the TMS are identical to the subsatellite of the TSS. In the numerical simulations, the atmospheric density is given as a function of the altitude above the Earth, which is approximated for the range from 100 to 500 km by using the 1976 Standard Atmosphere.[15] For the range higher than 500 km, the density is regarded to be negligible. Also, $r_E = 6378$ km and $\mu = 3.986 \times 10^{14}$ m^3/s^2 are used for Earth parameters.

Table 1 Parameters of subsatellites

Parameter	Value
M_s	100 kg
d_s	1.0 m
I_x, I_y, I_z	10 kg m^2
C_{ds}	2.0

Table 2 Parameters of tether

Parameter	Value
d_t	1.5 mm
$\sum M_t$	200 kg
$\sum l_n$	100 km
C_{dt}	2.0
E	5.0×10^9 N/m^2
Number of tether elements	20
k	1.77 N/m
c	0.25 N · s/m

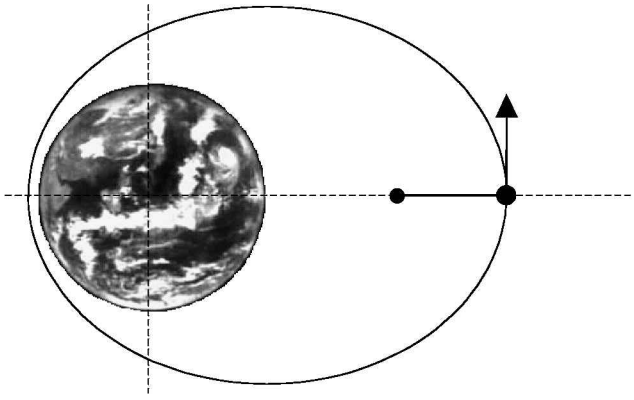

Fig. 5 Initial condition of tethered system.

Numerical Simulations

Initial Conditions

The initial conditions, which are $\psi_{T0} = 0$ and $\dot{\psi}_{T0} = 0$ relative to the orbital coordinate at the apogee (Fig. 5), are given in all simulations. Initial orbital parameters are given as follows:

$$r_0 = [(1+e)/(1-e)]r_{\text{peri}} \tag{27}$$

$$\dot{r}_0 = 0 \tag{28}$$

$$\nu_0 = \pi \tag{29}$$

$$\dot{\nu}_0 = \sqrt{(1-e)\mu/r_0^3} \tag{30}$$

Effect of Eccentricity

As mentioned before, the initial conditions and the eccentricity determine the motion of a tethered system, that is, whether it will tumble or librate. Orbital eccentricity causes changes of the orbital angular velocity and the gravity gradient, and its effect on the dynamic behavior is investigated through numerical simulations of the TSS neglecting the atmospheric drag. The altitude of perigee and the eccentricity are taken as $h_{\text{peri}} = 250$ km and $e = 0.2$. Numerical simulations have been carried out for 500 orbital revolutions. Numerical solutions are obtained by fourth-order Runge–Kutta method setting the time step at 0.1 s. By the variation of the size of the time step, the accuracy of the numerical results in the study is verified at least three significant digits at the end of the simulations.[16] To grasp the dynamic characteristics of libration of the total system, both the time-history of attitude angle and a Poincaré map are checked. A Poincaré map consists of discrete plots created by sampling the values of states periodically, which facilitates understanding of the changes in the motion characteristics of the system over long periods of time. In this study, $(x_s, \dot{x}_s)$ is mapped at every apogee point. Figure 6a is the Poincaré map, and Fig. 6b is the time history. The tether attitude angle ψ_T is obtained by the following equation:

$$\psi_T = \tan^{-1}(-x_s/y_s) \tag{31}$$

Plotted points in the Poincaré map form a closed curve, and in the time history, it is shown that the amplitude of libration continues to lie within fixed limits. From Fig. 6, it can be concluded that the tethered system continues quasi-periodic libration stably. It is known that the points are plotted at the center of the closed curve when the period of the libration is the same as one orbital period, which means periodic motion.[8] The frictional dissipation of the tether is expected to be effective in stabilizing the libration. However, the simulation of 500 revolutions does not verify its effect, and longer-term simulations are considered to be necessary to verify it. The deflection of the tether, the attitude motion of the subsatellite, and the tension of the tether element directly connected to the subsatellite in the numerical results are shown in Fig. 7. The deflection of the tether is defined as the difference between the stretched length

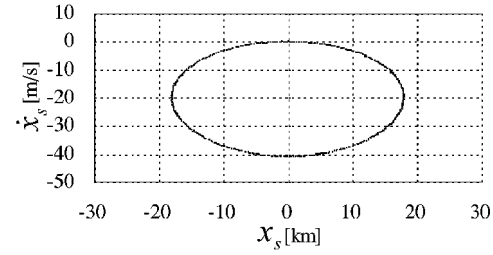

a) Poincaré map

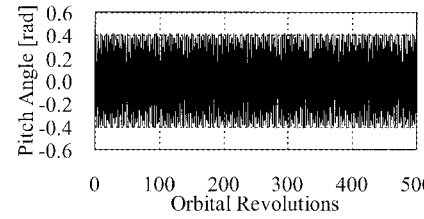

b) Time history

Fig. 6 Libration of tethered system; TSS ($h_{\text{peri}} = 250$ km).

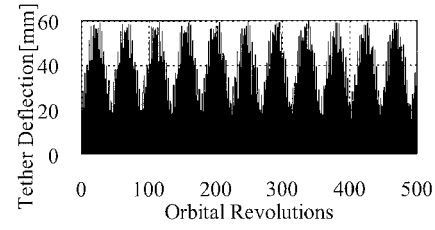

a) Deflection of tether

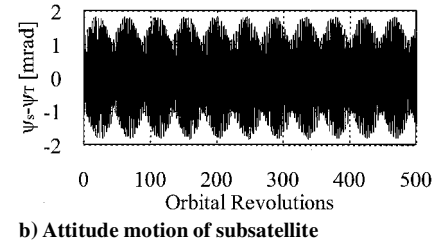

b) Attitude motion of subsatellite

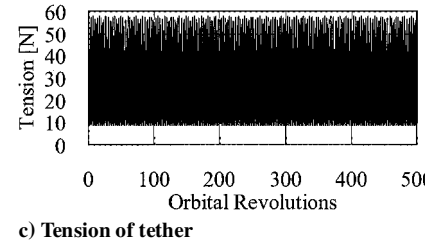

c) Tension of tether

Fig. 7 Dynamic response of tethered system neglecting atmospheric drag; TSS ($h_{\text{peri}} = 250$ km).

of the tether and the distance from the mother satellite to the subsatellite, which is expressed as

$$\Delta l = \sum l - \|\boldsymbol{x}_s\| \tag{32}$$

The attitude angle of the subsatellite is defined as the angle measured from the tether line, which is expressed as $\psi_s - \psi_T$. In Fig. 7, amplitudes of the attitude motion and the tension continue to stay within certain bounds, and it can be considered that these motions continue stably in the later duration.

It can be concluded that orbital eccentricity, where libration of the total system is possible, does not affect stability of the tethered system. To focus on the effect of atmospheric drag, the orbital eccentricity is set at $e = 0.2$, and many numerical results are obtained by letting h_{peri} vary as follows:

$$200 \leq h_{\text{peri}} \leq 300\,\text{km} \tag{33}$$

Effect of Atmospheric Drag on Libration

Numerical Results

In this section, the effects of atmospheric drag on libration are investigated. First, the set of equations of the TSS is integrated for 500 orbital revolutions in the orbits of $h_{\text{peri}} = 250$ km. The result is shown in Fig. 8. To understand the characteristics of the libration clearly, the durations from the 1st to the 100th revolution and from the 401st to the 500th revolution are focused on. In Fig. 8a, the points during revolutions 1–100 are denoted by circles, and those during revolutions 401–500 by crosses. The average radius of the crosses is obviously larger than that of the circles, and in the time history, the amplitude of the libration is getting larger. Comparison between Fig. 8 and Fig. 6 suggests that the libration diverges due to the effect of atmospheric drag.

Effect of Altitude of Perigee

To verify the effect of the altitude of perigee on the stability of libration, the rapidity of divergence can be taken as a kind of measure of the instability, and to evaluate the rapidity, a parameter λ is introduced by the following definition:

$$\lambda = \frac{1}{100}\left(\sum_{401}^{500} |x_s - x_{\text{sp}}| - \sum_{1}^{100} |x_s - x_{\text{sp}}|\right) \tag{34}$$

The approximate value of x_{sp} can be obtained as a mean value of x_s. The physical meaning of λ is the comparative measure of the approximate radius of plots in Poincaré map of revolutions 1–100 and the corresponding approximate radius of revolutions 401–500. When the libration diverges, λ has a positive value and vice versa. The result is shown in Fig. 9. In the unplotted cases, the total system begins tumbling within 500 orbital revolutions. In the case of

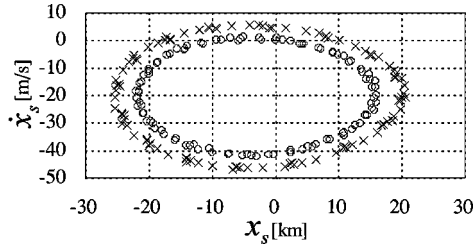

a) Poincaré map (○, revolutions 1–100 and ×, revolutions 401–500)

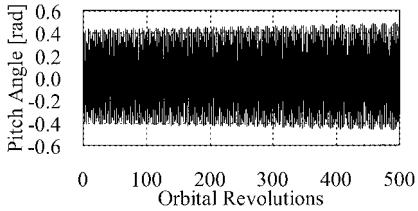

b) Time history

Fig. 8 Divergence of libration; TSS ($h_{\text{peri}} = 250$ km).

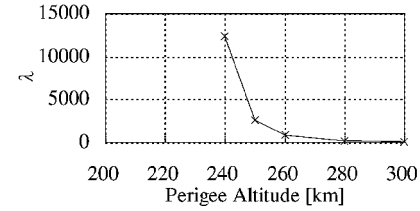

Fig. 9 Effect of altitude of perigee on λ; TSS.

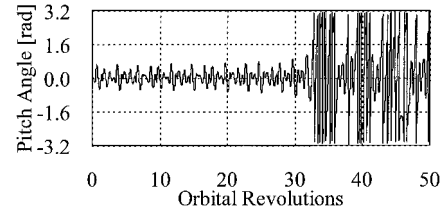

Fig. 10 Divergence of libration and tumbling motion; TSS ($h_{\text{peri}} = 220$ km).

$h_{\text{peri}} = 220$ km, the total system begins tumbling in the 32nd revolution. The change of the motion from libration to tumbling is shown in Fig. 10.

Physical Interpretation

If the motion of the tethered system is same as the periodic motion, libration never diverges. Therefore, the divergence can be interpreted by focusing on the deviation from the periodic motion. The angular velocity of libration of the tethered system in the inertial coordinate is $\dot{\nu} + \dot{\psi}_T$, and the centrifugal force of the tether is almost proportional to $(\dot{\nu} + \dot{\psi}_T)^2$. In the case of $\dot{\psi}_T < \dot{\psi}_{Tp}$, where the backward swing is slower than that of the periodic motion around the perigee, the centrifugal force diminishes, the tether becomes shorter, and the tethered system faces the atmosphere of lower density. Therefore, atmospheric drag on the system grows smaller than that of the periodic motion, and the slower backward swing is decelerated. Contrary, in the case of $\dot{\psi}_T > \dot{\psi}_{Tp}$, the tether elongates, the atmospheric drag is larger than that of the periodic motion, and the faster backward swing is accelerated. In this way, libration diverges from the periodic motion at every perigee. The lower altitude of perigee increases the instability because the atmospheric density and its gradient are larger. As mentioned before, in an elliptic orbit with a given orbital eccentricity, the initial condition determines whether the motion is in libration or tumbling motion. The region of the initial conditions, which lead a tethered system to continue libration, is distributed around the periodic motion in the Poincaré maps.[7–11] As the libration diverges from the periodic motion, the points are plotted outward in the Poincaré map, as shown in Fig. 8a. When a point is plotted outside of the libration region, the total system begins tumbling motion because of the changes of the orbital angular velocity and the gravity gradient. The physical interpretation can also be considered as follows: The effect of the atmospheric drag just results in the gradual changes, that is, divergence (Fig. 10; 0∼31 revolutions), and the changes of the orbital angular velocity and the gravity gradient give rise to the radical changes from the libration to the tumbling motion (Fig. 10; after 32 revolutions).

Effect of Atmospheric Drag on Tension State of Tether and Attitude Motion of Subsatellite

Numerical Results

In this section, the effects of atmospheric drag on tension state of the tether and attitude motion of the subsatellite are investigated. Tension and deflection of the tether and attitude motion of the subsatellite are focused on. At first, the motion of the tethered system in the case of $h_{\text{peri}} = 250$ km is checked. Figures 11a–11c are the time histories of the tether deflection, attitude motion of the subsatellite, and tension of the tether element connected to the subsatellite. When these figures are compared with Fig. 7, it is obvious that the deflection and the attitude motion are excited significantly by the atmospheric drag.

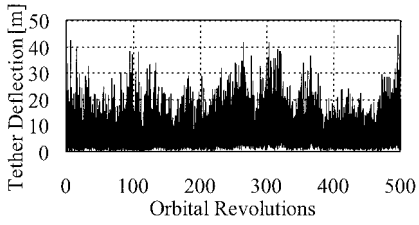

a) Deflection of tether

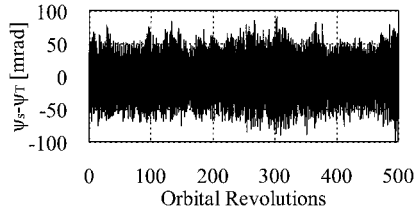

b) Attitude motion of subsatellite

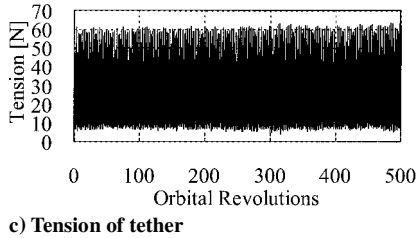

c) Tension of tether

Fig. 11 Dynamic response of tethered system considering atmospheric drag; TSS (h_{peri} = 250 km).

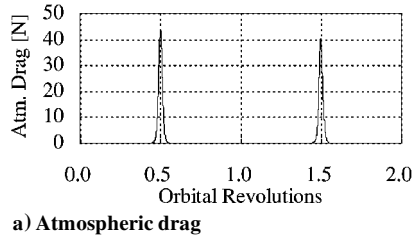

a) Atmospheric drag

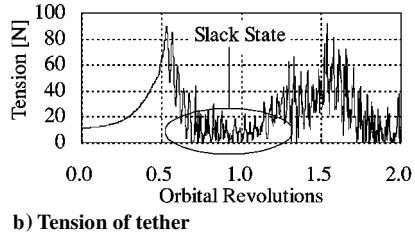

b) Tension of tether

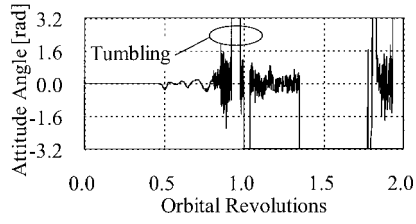

c) Attitude motion of subsatellite

Fig. 12 Dynamic response of tethered system with large atmospheric drag; TSS (h_{peri} = 220 km).

Slack State of Tether

The numerical result in the case of $h_{peri} = 220$ km is rearranged, where the total system begins tumbling during the 32nd revolution, as shown in Fig. 10. The time histories of the atmospheric drag on the total system, tension of the tether element, and attitude motion of the subsatellite during the beginning two revolutions are shown in Fig. 12. In this case, the tether element goes slack due to the impulsive atmospheric drag around the first perigee, and the subsatellite begins unstable motion. The tether in a slack state does not provide any tension to the subsatellite, and the system shows abrupt change of attitude motion. The subsatellite behaves unstably, which emerges as in-plane tumbling motion as shown in Fig. 12c. This result means that the slack state of the tether is inevitable in the orbits of lower perigee, and the subsatellite is perturbed significantly even if the total system continues libration.

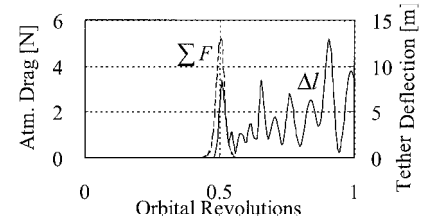

a) Atmospheric drag and tether deflection

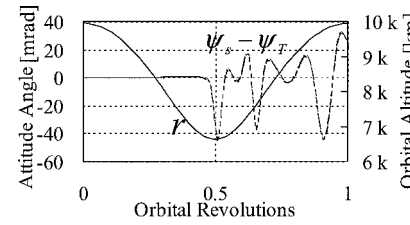

b) Attitude motion and orbital altitude

Fig. 13 Detailed aspects of tethered system during first revolution; TSS (h_{peri} = 250 km).

Physical Interpretation

The time histories of the atmospheric drag on the total system $\sum F$, deflection of the tether Δl, and attitude motion of the subsatellite during the beginning first revolution are shown in Fig. 13. From Fig. 13, physical interpretation of the excitation can be obtained: The atmospheric drag causes the deflection of the tether, and the lateral vibration of the tether excites the attitude motion of the subsatellite. In the orbits of lower perigee, the tether elements in the lower positions face larger atmospheric drag, and the amplitude of the difference of the tether tension from the nominal one (without atmospheric drag) becomes large as shown in Fig. 12b (around 0.5 revolution). When the perigee is lower than a certain altitude, the smallest value of the tether tension can be nothing around the apogee, where the nominal tension is minimum. In this case, the tether tension can have a large value just after the slack states. Such radical changes of the tether tension repeats for a certain duration, circled in Fig. 12b, which can be a large perturbation for the attitude motion of the subsatellite.

Dynamic Behavior of TMS

The divergence of libration is also observed in the case of TMS. The pitch angle of the tether is obtained by substituting x_d for x_s and y_d for y_s, respectively, in Eq. (31). The result in the case of $h_{peri} = 250$ km is shown in Fig. 14, and it is obvious that the libration diverged more rapidly than it did for the TSS shown in Fig. 8. In the case of $h_{peri} = 240$ km, the total system begins tumbling during the 396th revolution, as shown in Fig. 15a. In Fig. 15b, T_a–T_d denote the tension of the tether elements, which are connected to subsatellites a–d, respectively. As shown in Figs. 15b and 15c, the tether elements of the whole system go slack just before the total system begins tumbling, and all subsatellites behave unstably. In this case, the amplitude of the libration is so large that the gravity-gradient effect is not large enough to maintain the tension of the tether. Therefore, all tether elements go slack at almost same time. The dynamic response in the case of $h_{peri} = 220$ km is shown in Fig. 16. In this case, impulsive atmospheric drag significantly perturbs the tethered system. Slack states occur more frequently in the lower tether elements, and the subsatellites in the lower positions of the system tend to behave unstably. This result shows that partial instability of the system can occur in TMSs.

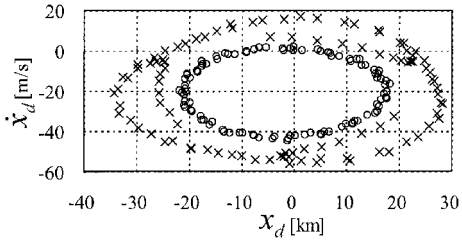

a) Poincaré map (○, revolutions 1–100 and ×, revolutions 401–500)

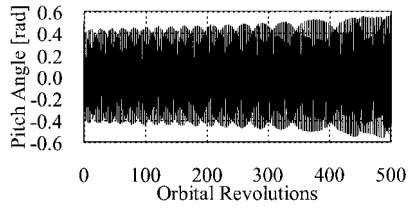

b) Time history

Fig. 14 Divergence of libration; TMS (h_{peri} = 250 km).

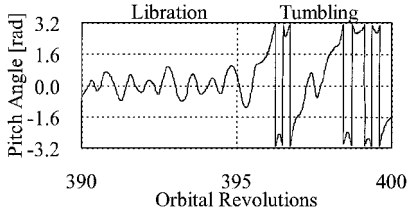

a) Change of motion

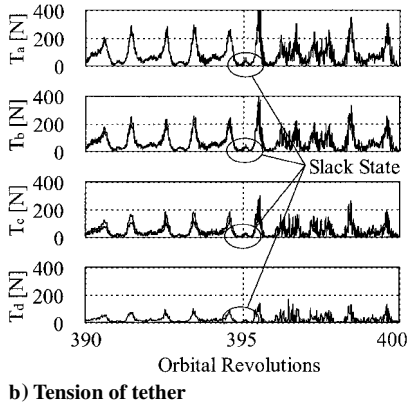

b) Tension of tether

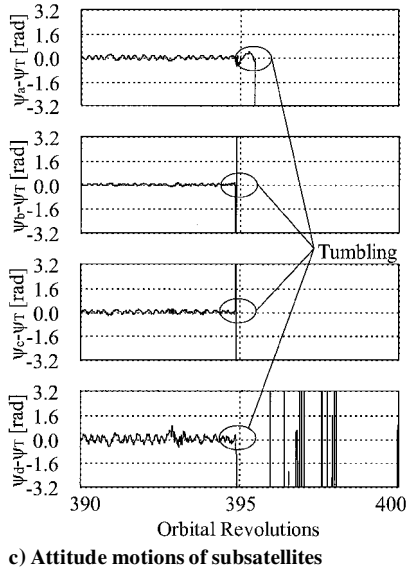

c) Attitude motions of subsatellites

Fig. 15 Dynamic response of tethered system with tumbling motion; TMS (h_{peri} = 240 km).

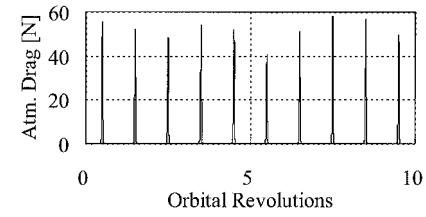

a) Atmospheric drag on total system

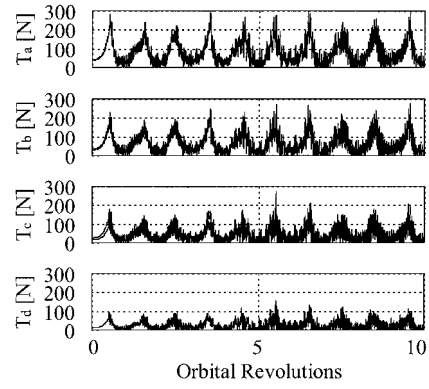

b) Tension of tether

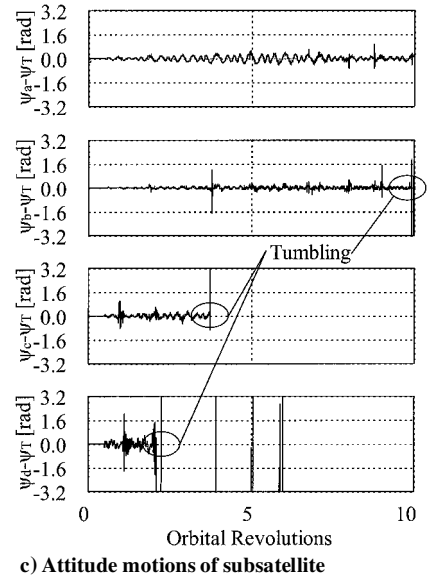

c) Attitude motions of subsatellite

Fig. 16 Dynamic response of tethered system with large atmospheric drag; TMS (h_{peri} = 220 km).

Conclusions

Dynamic behavior of tethered systems in elliptic orbits is investigated through numerical experiments. The mathematical model of the tethered system includes distributed mass and flexibility of the tether, rigid-body motions of the subsatellites, and atmospheric drag. Through Poincaré maps and time histories, physical interpretations of dynamic behavior are clearly shown.

Concerning the libration of the total system, numerical results have shown that the libration of the total system can be unstable due to atmospheric drag, that unstable librations diverge from the nominal periodic motion, and that later total systems begin tumbling. Because both the atmospheric density and its gradient increase as the altitude becomes lower, the instability of librations increases in the orbits of lower altitude of perigee. Concerning tension states of the tether and attitude motions of the subsatellites, the physical interpretation is obtained from the numerical results: Atmospheric drag causes deflection of the tether, and lateral vibration of the tether significantly perturbs attitude motions of the subsatellites. Slack states of the tether are focused on, and it has been shown that they occur both when the total system begins tumbling and when the

tethered system faces impulsive atmospheric drag in the orbits of lower altitude of perigee. The tether in a slack state does not restrain the motions of the subsatellites, and this allows the motions of the subsatellites to be perturbed significantly. In the TMS case, the large perturbations can partially cause the slack states of the tether, which causes unstable attitude motions of some of the subsatellites.

It can easily be considered that many other results can be obtained for tethered systems of other system configurations, such as the length, diameter, and material of the tether, shapes and masses of the subsatellites, and orbital parameters. Therefore, the effects of the system configurations on the stability should be clarified in future work. Furthermore, active control of the libration motion should also be considered.

References

[1]Oyama, K. I., Sasaki, S., Su, Y., and Balan, N., "Feasibility Study on a Tethered Satellite System," *Proceedings of 2nd International Workshop on the Application of Tethered Systems in Space*, Inst. of Space and Astronautical Science, Kanagawa, Japan, 1994, pp. 325–334.

[2]Beletskii, V. V., and Levin, E. M., "Dynamics of the Orbital Cable System," *Acta Astronautica*, Vol. 12, No. 5, 1985, pp. 285–291.

[3]Onoda, J., and Watanabe, N., "Tethered Satellite Swinging from Atmospheric Gradient," *Journal of Guidance, Control, and Dynamics*, Vol. 11, No. 5, 1988, pp. 477–479.

[4]de Matteis, G., and de Socio, L. M., "Dynamics of a Tethered Satellite Subjected to Aerodynamic Forces," *Journal of Guidance, Control, and Dynamics*, Vol. 14, No. 6, 1991, pp. 1129–1135.

[5]de Matteis, G., "Dynamics of a Tethered Satellite in Elliptic, Nonequatorial Orbits," *Journal of Guidance, Control, and Dynamics*, Vol. 15, No. 3, 1992, pp. 621–626.

[6]Modi, V. J., and Brereton, R. C., "Periodic Solutions Associated with the Gravity-Gradient-Oriented System: Part I. Analytical and Numerical Determination," *AIAA Journal*, Vol. 7, No. 7, 1969, pp. 1217–1225.

[7]Modi, V. J., and Brereton, R. C., "Periodic Solutions Associated with the Gravity-Gradient-Oriented System: Part II. Stability Analysis," *AIAA Journal*, Vol. 7, No. 8, 1969, pp. 1465–1468.

[8]Karasopoulos, H. A., and Richardson, D. L., "Chaos in the Pitch Equation of Motion for the Gravity-Gradient Satellite," AIAA Paper 92-4369, Aug. 1992.

[9]Karasopoulos, H. A., and Richardson, D. L., "Numerical Investigation of Chaos in the Attitude Motion of a Gravity-Gradient Satellite," American Astronautical Society, AAS Paper 93-581, Aug. 1993.

[10]Nixon, M. S., and Misra, A. K., "Nonlinear Dynamics of Two-Body Tethered Satellite Systems," American Astronautical Society, AAS Paper 93-731, Aug. 1993.

[11]Fujii, H. A., and Ichiki, W., "Nonlinear Dynamics of the Tethered System in the Station Keeping Phase," *Journal of Guidance, Control, and Dynamics*, Vol. 20, No. 2, 1997, pp. 403–406.

[12]Humble, R. W., "Two Dimensional Tethered Satellite Attitude Dynamics," *Journal of the Astronautical Sciences*, Vol. 38, No. 1, 1990, pp. 21–27.

[13]Bergamaschi, S., and Bonon, F., "Coupling of Tether Lateral Vibration and Subsatellite Attitude Motion," *Journal of Guidance, Control, and Dynamics*, Vol. 15, No. 5, 1992, pp. 1284–1286.

[14]Santangelo, A. D., "Optimal Attitude Control of a Tethered End Mass in the Earth's Upper Atmosphere," AIAA Paper 97-0355, Jan. 1997.

[15]*U.S. Standard Atmosphere*, U.S. Government Printing Office, Washington, DC, 1976.

[16]Davis, G. V., *Numerical Methods in Engineering and Science*, Allen and Unwin, London, 1986, pp. 176–179.

C. A. Kluever
Associate Editor